

Orbach Relaxation and Hyperfine Structure in the Excited $\bar{E}(^2E)$ State of Cr^{3+} in Al_2O_3

S. GESCHWIND, G. E. DEVLIN, R. L. COHEN, AND S. R. CHINN

Bell Telephone Laboratories, Murray Hill, New Jersey

(Received 28 September 1964)

Several methods of optical detection of electron paramagnetic resonance (epr) of excited states in crystals are outlined. The application of these methods to observation of epr in the excited metastable $\bar{E}(^2E)$ state of Cr^{3+} in Al_2O_3 is described. The most recent technique made use of a high-resolution optical spectrometer to monitor the change of intensity of one of the Zeeman components of the R_1 fluorescent light [$\bar{E}(^2E) \rightarrow ^4A_2$] as \bar{E} was saturated by the microwaves when the magnetic field was swept through resonance. A sample doped with Cr enriched to 92% Cr^{53} was used to study the hfs in the \bar{E} state. An upper limit of 25 kG is set on the hyperfine field per unit spin ($A/gI\beta_N$). This small value compared to that of 200 kG for the ground-state results from a near cancellation of the negative core polarization field by an equally large but positive orbital field. The spin-lattice relaxation time T_1 in the \bar{E} level was determined by observing the recovery of the light signal after the microwave saturating pulse was switched off. A continuous averaging technique using a multichannel analyzer was employed to improve the signal-to-noise ratio. T_1 is found to very accurately follow an Orbach process with $T_1 = 3.8 \times 10^{-9} e^{\Delta/kT}$ sec where $\Delta = 28.8 \pm 1.0 \text{ cm}^{-1}$, i.e., the separation between $2\bar{A}$ and \bar{E} . In the range of temperature where the Orbach process was observed ($4.2^\circ\text{K} \rightarrow 2.8^\circ\text{K}$), T_1 was found to be essentially independent of concentration (0.05 and 0.005%) and frequency (24 and 48 kMc/sec), as anticipated. The coefficient 3.8×10^{-9} sec is significant in that it measures the maximum transition time from $2\bar{A}$ to \bar{E} , $T_{2\bar{A} \rightarrow \bar{E}}$, with spontaneous emission of a 29-cm^{-1} phonon. This time plays an important role in considering the production of 29-cm^{-1} acoustic phonons by the pumping light. Initial evidence is cited for the generation by the pumping light of a narrow-band "hot-phonon" spike at 29 cm^{-1} as seen by the spin-lattice relaxation in the \bar{E} level.

I. INTRODUCTION

IN recent years there has been a growing interest in a detailed examination of excited states of magnetic impurity ions in crystals. Specifically, it would be desirable to study these excited levels with the high resolution of electron paramagnetic resonance which has been so successfully applied to the study of ground states. In the attempt to detect the microwave absorption directly in the excited states one is generally hampered by the fact that the number of ions that can be maintained in these excited states by the usual methods, such as optical excitation, is far too small; i.e., the combination of the relevant factors such as pumping power available, optical absorption factor, and lifetime of the excited state are such as to yield a number of ions in the excited state below the limiting sensitivity of conventional epr techniques.¹ However, if the excited state in question is fluorescent, one can seek to monitor a change in the fluorescent light from this level when the microwave frequency coincides with its Zeeman splitting, rather than monitor the absorption of microwave power. As one is detecting optical rather than microwave photons, orders of magnitude sensitivity may be achieved. This would be the analog in solids of the optical rf double resonance techniques first suggested by Brossel and Kastler² and widely used

in gases as, for example, first applied by Bitter and Brossel³ to the 3P_1 sublevels of Hg.

Within the general framework of optical detection of microwave absorption in excited states in solids three methods immediately suggest themselves and are illustrated by reference to Fig. 1. For the purposes of illustrating these different methods, consider an excited state doublet which is maintained in a steady state by some continuous pumping means and which decays by fluorescence to a ground doublet. Assume that both doublets are split in a magnetic field and have selection rules as shown. Further assume that there is a thermalization of a certain degree or that if necessary some selective means of filling levels a and b has been used so that the population of level a , n_a , is less than that of b , n_b .

Method 1. Circular Polarization

If we look along the direction of magnetic field, the intensity of the left-circular component of light (line A) will be less than the right-circular component (line B) since $n_a < n_b$. If one therefore monitors with appropriate polarizers the light along the dc magnetic field, one will observe an increase in left-circularly polarized light and a decrease in right-circularly polarized light as microwave transitions are induced at the resonance between levels a and b , due to the increase in n_a and decrease in n_b .

Note that the Zeeman splitting need not be resolved at all in this method, i.e., the linewidths may be considerably greater than the splitting. However, as far as

¹ To the extent that we are solely concerned with impurity ions in essentially ionic crystals, these remarks are generally valid. They do not apply to excited triplet states of organic crystals which are so long-lived (one second or greater) that one can easily produce sufficient excited centers so that, they can be observed by direct microwave absorption. B. A. Hutchison, Jr., and B. W. Mangum, *J. Chem. Phys.* **34**, 908 (1961).

² J. Brossel and A. Kastler, *Compt. Rend.* **229**, 1213 (1949).

³ J. Brossel and F. Bitter, *Phys. Rev.* **86**, 308 (1952).

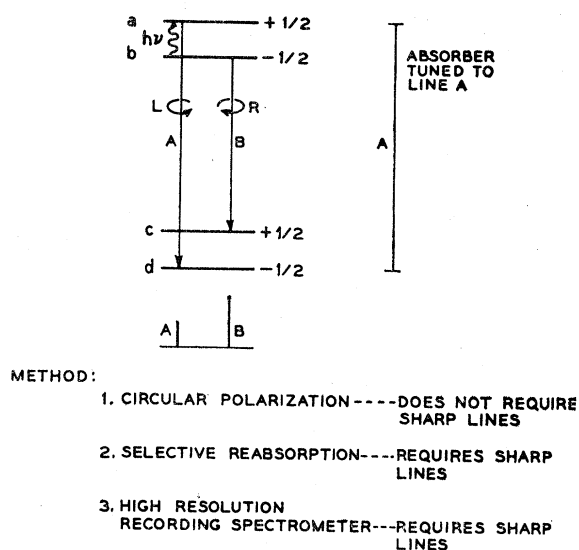


FIG. 1. Illustration of optical detection of epr in an excited state. ab is the hypothetical excited-state doublet which fluoresces to the ground-state doublet cd . It is assumed that the population of level b is greater than that of a as a result of either thermalization in the excited state or selective filling. $h\nu$ indicates an induced microwave transition.

solids are concerned this method of circular polarization has several disadvantages. For one, it requires looking along the direction of the field, which could prove experimentally inconvenient where one is pressed for space between pole faces of a magnet with a microwave cavity inside a double Dewar arrangement for low-temperature work. In addition, for other than cubic crystals, one must not only view along the field direction but the dc field must be along the unique axis of the crystal for the light to be completely circularly polarized. This limits one's attempt to study the epr spectrum of the excited state with the magnetic field in any arbitrary direction relative to the unique axis. None of these latter objections can really be considered as overriding considerations, but in any case no excited state epr has been done as yet in a *solid* by monitoring a change in circularly polarized light.

Method 2. Selective Reabsorption

Imagine that the *total* fluorescent light is viewed after being passed through a material that selectively absorbs line A . Then in effecting a microwave transition from b to a , light which was previously emitted in line B will now be emitted in line A which is more strongly attenuated by the absorber, so that the total light $A+B$ reaching the viewer will be decreased. The absorber in question need not be external to the fluorescent system. For example, lines A and B may have sufficient oscillator strength and enough centers may be present in the ground state so that A and B are internally reabsorbed in the sample. Reabsorption will decrease the intensity of emitted radiation from the

sample as one may assume the existence of nonradiative decay to the ground state as well as the more probable decay by radiative transition. If, in addition, one is at sufficiently low temperature such that $n_d > n_c$, then A will be more strongly reabsorbed than B . If one now induces a microwave transition from b to a , then again the total light ($A+B$) viewed in a given direction (which now may be arbitrary and, for example, in the more convenient direction at right angles to the external magnetic field) will be found to decrease due to this selective reabsorption.

This method of selective reabsorption has been used in gases.⁴ It was applied successfully for the first time in a solid in the initial epr study of the excited metastable $\bar{E}(^2E)$ of Cr^{3+} in Al_2O_3 reported earlier,⁵ following the study of this reabsorption by Varsanyi, Wood, and Schawlow.⁶ However, such large internal reabsorption as is present in ruby is not so easily achieved in other cases, as for example in V^{2+} and Mn^{4+} in Al_2O_3 , which are under study, or in exceedingly dilute ruby (parts per million of Cr). In general therefore factors such as smaller available concentrations of the impurity ion, reduced oscillator strength and broader optical lines will reduce the reabsorption. In addition, at higher temperatures, levels c and d of the ground state are more nearly equally populated and the reabsorption becomes less selective between lines A and B . In ruby, for example, a significant decrease in signal-to-noise, S/N , was observed as one went from 1.6 to 4°K, due to the decrease in selective reabsorption. This led to the adoption of method 3 described in the next paragraph.

Method 3. Use of High-Resolution Optical Spectrometer

Assume that the Zeeman splitting between A and B can be resolved with a high-resolution optical scanning spectrometer. Then one may sit on line A and monitor its intensity with a photocell. If a microwave transition is induced between b and a , thereby increasing the population of a , one will observe an increase in the photocell output. It is this latter that we have found most useful in studying the epr and specifically the spin-lattice relaxation time between the Zeeman components of the excited $\bar{E}(^2E)$ state of ruby.

II. ENERGY LEVEL SCHEME OF Cr^{3+} IN Al_2O_3

We briefly review the very well known energy level scheme of Cr^{3+} in Al_2O_3 with the aid of Fig. 2.⁷ The free-ion ground state is 4F with $L=3$ and $S=\frac{3}{2}$. The

⁴ H. Bucka, *Naturwiss.* **43**, 371 (1956); H. Bucka, *Z. Physik* **151**, 328 (1958). R. H. Kohler, *Phys. Rev.* **121**, 1104 (1961).

⁵ S. Geschwind, R. J. Collins, and A. L. Schawlow, *Phys. Rev. Letters* **3**, 544 (1959); S. Geschwind, in *Magnetic and Electric Resonance and Relaxation Proceedings of Colloque Ampere, Eindhoven, July 1962*, edited by J. Smidt (Interscience Publishers, Inc., New York, 1963), p. 548.

⁶ F. Varsanyi, D. L. Wood, and A. L. Schawlow, *Phys. Rev. Letters* **3**, 545 (1959).

⁷ S. Sugano and Y. Tanabe, *J. Phys. Soc. Japan* **13**, 880 (1958).

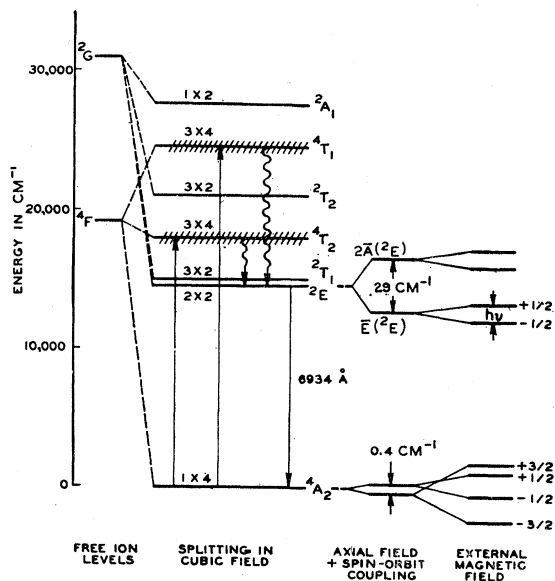


FIG. 2. Partial energy-level diagram of Cr^{3+} in Al_2O_3 in an external magnetic field.

sevenfold orbital degeneracy is split in a cubic field into a 4A_2 orbital singlet and the 4T_2 and 4T_1 triplets which are shown cross-hatched and are the main absorption bands of ruby. The famous fluorescent 2E state arises primarily from the free ion 2G level but at the strength of cubic crystal field in ruby is, of course, an admixture of many of the free-ion doublet states, i.e., 2G , 2D , 2H , 2P . The splitting of the 2G level in a cubic field is also shown.⁸ The strength of the cubic crystal field is such that the 2E level falls below the 4T_2 and 4T_1 levels. The 2E is populated by the ion-absorbing light in the green and blue, corresponding to the $^4A_2 \rightarrow ^4T_2$ and $^4A_2 \rightarrow ^4T_1$ transitions, and subsequent decay by radiationless transitions to the 2E level. The quantum efficiency of this fluorescence is of order unity⁹ (anywhere from 50 to 90%). In addition to the predominant cubic field there is also present a smaller trigonal field which in combination with the spin-orbit coupling splits the 4A_2 ground state by 0.4 cm^{-1} and the 2E state into two Kramers doublets separated by approximately 29 cm^{-1} . It is in the lower of these doublets, i.e., in the $\bar{E} (^2E)$ that epr is performed. Figure 3(a) extracts from Fig. 2 that portion of the diagram most pertinent to the experiment. The selection rules for the optical transitions between the \bar{E} and the 4A_2 states with the external magnetic field along the c axis have been worked out by Sugano and Tanabe⁷

⁸ The apparent nonconservation of center of gravity of the levels split off from the 2G level is due to the fact that these crystal field states are admixtures of many other free-ion states and one must consider the conservation of the center of gravity of all the levels combined, many of which are not shown.

⁹ T. H. Maiman, Phys. Rev. Letters 4, 564 (1960); T. H. Maiman, R. H. Hoskins, I. J. D'Haenens, C. K. Asawa, and V. Evtuhov, Phys. Rev. 123, 1151 (1961).

and are shown in Fig. 3(a) for the σ polarized light ($E \perp c$). The π components ($E \parallel c$) are considerably weaker and are discriminated against by the optical spectrometer so that they have been omitted. (These selection rules have been largely verified in experimental studies of the optical Zeeman spectrum of ruby by Sugano and Tsujikawa¹⁰ and Sugano, Aoyagi, and Misu.¹¹) A steady-state population is maintained in \bar{E} by continuous excitation to the absorption bands with mercury light. Epr in \bar{E} is observed using method 3 outlined above by monitoring the change in the intensity of line A with a high-resolution spectrometer.

There are no matrix elements, diagonal or off-diagonal, of spin-orbit coupling or trigonal field within the 2E level. The trigonal field $V \propto (xy + yz + xz)$ transforms as the T_2 irreducible representation of the cubic group, and since the direct product $E \times E = A_1 + A_2 + E$ does not contain T_2 there are no matrix elements of trigonal field within E . Similarly, the angular momentum \mathbf{L} transforms as a vector or as the T_1 representation so that in addition there are no matrix elements of spin-orbit coupling within E . However $T_2 \times T_1$ does contain E so that in second order the combined action of the trigonal field and spin-orbit coupling splits the E level into two Kramers doublets separated by a distance Δ given by⁷

$$\Delta = \frac{\langle ^2E | V_{\text{trig}} | ^2T_2 \rangle \langle ^2T_2 | \sum_i \zeta \mathbf{l}_i \cdot \mathbf{s}_i | ^2E \rangle}{W(^2E) - W(^2T_2)}, \quad (1)$$

restricting oneself to admixed terms of the t_2^3 con-

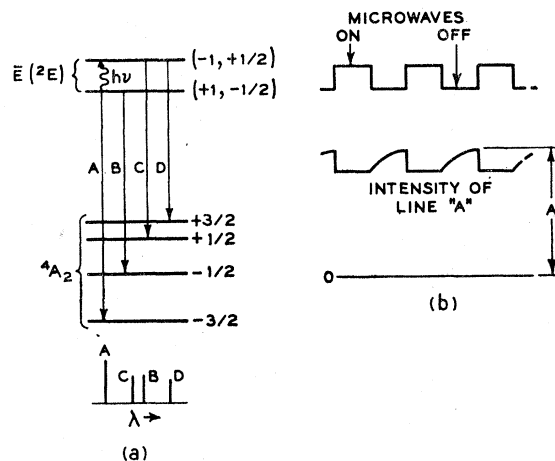


FIG. 3. (a) σ components of R_1 light [$\bar{E} (^2E) \rightarrow ^4A_2$] with H_{ext} along the c axis. The two π components have been omitted as they are weaker and are discriminated against by the grating of the spectrometer. (b) Decrease of intensity of line A as ions are transferred from $(+1, -\frac{1}{2})$ to $(-1, +\frac{1}{2})$ and subsequent recovery due to spin-lattice relaxation and radiation to ground state. Sample is continuously irradiated with Hg light.

¹⁰ S. Sugano and I. Tsujikawa, J. Phys. Soc. Japan 13, 899 (1958).

¹¹ K. Aoyagi, A. Misu, and S. Sugano, J. Phys. Soc. Japan 18, (1963).

figuration only. Evaluation of (1) gives

$$\Delta = \frac{4K\zeta}{W(^2E) - W(^2T_2)}, \quad (2)$$

where K is the trigonal field parameter and ζ the one-electron spin-orbit (s-o) coupling parameter. In a magnetic field, the Kramers doublets are split with first-order eigenfunctions as labeled in Fig. 4. Here the $\pm\frac{1}{2}$ are the spin quantum numbers and ± 1 is an orbital quantum number describing the transformation properties of the wave functions under rotation around the axis of quantization which is taken to be the trigonal axis of the crystal.

Since no matrix elements of \mathbf{L} exist within E one would expect a g_{11} for the \bar{E} and $2\bar{A}$ levels corresponding to spin only, i.e., $g_{11} \approx 2.0023$. Moreover, since the spin operator cannot affect the orbital quantum number, transitions between the Zeeman components of \bar{E} or $2\bar{A}$ would be forbidden to first order, i.e.,

$$g_{11} = 2 \langle ^2E(\mp\frac{1}{2}, \pm 1) | L_z + 2S_z | ^2E(\mp\frac{1}{2}, \pm 1) \rangle = 2, \quad (3)$$

$$g_{11} = 2 \langle ^2E(-\frac{1}{2}, +1) | \mathbf{L} + 2\mathbf{S} | ^2E(+\frac{1}{2}, -1) \rangle = 0. \quad (4)$$

Sugano and Tanabe⁷ have shown that higher order processes involving V_{trig} mix in some orbital angular momentum from the 2T_1 and 2T_2 states into the 2E to give a $g_{11}(\bar{E}) \approx 2.4$ and $g_{11}(2\bar{A}) \approx 1.6$. In addition, Clogston¹² has shown how a whole series of higher order processes involving V_{trig} , $V_{\text{s-o}}$ and V_{Coul} give rise to a small $g_{11} \approx 0.06$. The experimentally observed upper limit for g_{11} is ≈ 0.06 .

It is important to keep in mind these higher order modifications of the 2E states for several reasons. First, since g_{11} of the \bar{E} is not identically zero, microwave transitions between its Zeeman components will be allowed. However, as g_{11} is so small, one will require microwave power levels much larger than normally needed to saturate most paramagnetic transitions at low temperatures. Secondly, the departure of g_{11} from

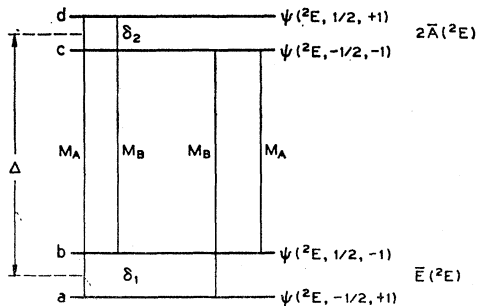


FIG. 4. Zero-order designation of \bar{E} and $2\bar{A}$ states. Δ is approximately 29 cm^{-1} . M_B refers to a nonspin-flip matrix element for phonon emission from $2\bar{A}$ to \bar{E} without a spin change, while M_A refers to a spin flip. $M_B < M_A$.

¹² A. M. Clogston, Phys. Rev. **118**, 1229 (1960).

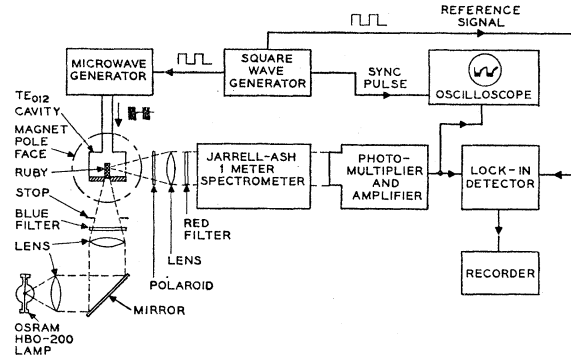


FIG. 5. Block diagram of system used for optical detection of epr in the $\bar{E}(^2E)$ excited state of ruby.

2.0023 measures the admixed orbital angular momentum and will have a bearing on the hyperfine field in this state.

Finally, as concerns spin-lattice relaxation, since neither E nor T_2 vibrations couple to $^2E(t_2^3)$, the $^2E(t_2^3)$ has no direct interaction with the lattice, one must go outside this state to effect spin-lattice relaxation. Moreover, we will have occasion later to consider the transition from $2\bar{A}$ to \bar{E} with spontaneous emission of a 29-cm^{-1} phonon. Actually, there will be four such phonons which differ from each other by roughly the Zeeman energy. Two of these transitions will involve a spin flip (M_A) and the other two are nonspin flip (M_B) as shown in Fig. 4. Since the very existence of these radiationless transitions depends upon the mixing into 2E of some of the 2T_2 state by spin-orbit interaction and trigonal field, the relative ratio of the spin-flip and nonspin-flip transitions is not readily apparent and will depend on the details of this mixing.

III. EXPERIMENTAL PROCEDURE

The experimental arrangement used is shown in Fig. 5. The ruby samples varied in size from $\frac{1}{16}$ to $\frac{1}{8}$ in. in diameter and approximately $\frac{3}{8}$ in. in length. The c axis was at right angles to the cylinder axis and normally parallel to the magnetic field. The sample is mounted vertically along the axis of a microwave cavity operating in the TE_{012} mode. It is continuously illuminated by a 250-W Osram mercury lamp through a small hole in the bottom of the cavity. A Corning glass filter is used to cut out red light from the mercury lamp. The fluorescent radiation is viewed at right angles to the field through horizontal slots cut in the cavity which do not interfere with current flow in this mode. A particular Zeeman component of the R_1 light is selected by the high-resolution 1-m Ebert scanning spectrometer.¹³ It is monitored by an RCA 7326 photomultiplier or a cooled RCA 7102. At K band, the microwave generator

¹³ Manufactured by Jarrell-Ash Company. A Harrison grating of 7620 lines per inch blazed for operation around 55° is used in eighth order giving a resolving power of over 250 000 in this region.

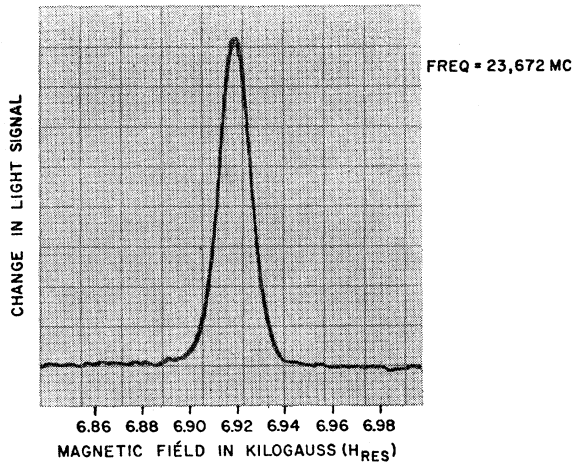


Fig. 6. Epr signal observed by optical detection in \bar{E} at 1.6°K from approximately 10^{11} spins in \bar{E} .

used was a 2K33 klystron while at 48 kMc/sec a BTL backward wave oscillator was used. Each tube had a maximum power output of approximately 40 mW. The microwave generator was amplitude modulated with a low-frequency square wave (20 to 400 cps) so that the small percentage change in light intensity of a selected Zeeman component, which occurs as the magnetic field moves through resonance in \bar{E} , is modulated at this frequency. This signal is then fed through a lock-in detector and on to a pen recorder. An illustration of the signal to noise obtained by this technique is shown in Fig. 6 where it is estimated that there were approximately 10^{11} ions in $\bar{E} (^2E)$. Note that the epr linewidth of approximately 16 G is orders of magnitude less than the width of the \bar{E} level ($\approx 0.1 \text{ cm}^{-1}$ or 1-kG) which is due to inhomogeneous crystal-field broadening.

At temperatures below the λ point of helium the change in light signal was large enough compared to noise that the resonance could be observed directly on the oscilloscope without the need for the narrow-banding techniques of lock-in detection.

IV. HYPERFINE STRUCTURE IN $\bar{E} (^2E)$ STATE

The essential spectroscopic results of the \bar{E} level were presented earlier⁵ and are well represented by the spin Hamiltonian

$$\mathcal{H}_C = g_{11}\beta H_z S_z + g_{\perp}\beta(H_x S_x + H_y S_y), \quad (5)$$

with $g_{11} = 2.445$ and $g_{\perp} \leq 0.06$.

To these earlier results we now wish to add the magnetic hyperfine interaction of the Cr^{53} nucleus in the $\bar{E} (^2E)$ state. This interaction is represented by an additional term

$$\mathcal{H}_{CN} = A_{11}I_z S_z + A_{\perp}(I_x S_x + I_y S_y). \quad (6)$$

Because g_{\perp} was so close to zero we could not determine A_{\perp} but only A_{11} .

A sample of Al_2O_3 containing 0.1% Cr enriched to 92% Cr^{53} was grown from the flux by Remeika. In Fig. 7(a) is shown the hyperfine structure splitting of the $-\frac{1}{2} \rightarrow +\frac{1}{2}$ transition of the 4A_2 ground state for which A_{11} is known to be $16.80 \pm 0.04 \times 10^{-4} \text{ cm}^{-1}$.^{14,15} In Fig. 7(b) is shown the $(-\frac{1}{2}, +1) \rightarrow (+\frac{1}{2}, -1)$ transition in the \bar{E} state in the same isotopically enriched crystal with no hfs apparent. From the width of this line in the unenriched crystals we may put an upper limit on $A_{11}(\bar{E}) < 2.0 \times 10^{-4} \text{ cm}^{-1}$ which corresponds to a field per unit electron spin at the Cr nucleus of $< 25 \text{ kG}$ in contrast with $-202\,000$ in the ground state. This result is easily understood in terms of the near cancellation of the orbital hyperfine field with the core polarization field in the \bar{E} state. The hyperfine field in the 4A_2 ground state is essentially due to core polarization, i.e., of the total hyperfine field of $-202\,000 \text{ G}$ per unit spin only some -7000 G is contributed by orbital and dipolar fields, so that we may adopt a figure of $-195\,000 \text{ G}$ for the core polarization field for $3d^3$.¹⁶ However, as indicated by the g shift in \bar{E} there is a not inconsiderable admixture of orbital angular momentum which would lead to a large orbital hyperfine (h.f.) field. The

92% ENRICHED Cr^{53} IN Al_2O_3 ($\text{Cr}:\text{Al} \sim 1:10^3$)

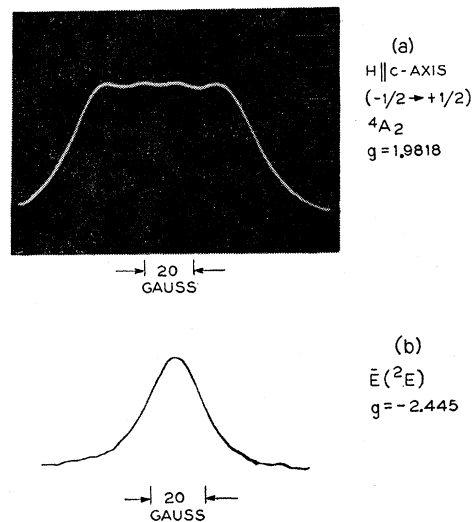


Fig. 7. Top figure shows epr signal from $-\frac{1}{2} \rightarrow +\frac{1}{2}$ transition of 4A_2 ground state in sample enriched with Cr^{53} . The hyperfine constant is approximately 20 G (separation between h.f. components). Lower figure shows resonance observed in same sample with no resolved hfs apparent. One may place an upper limit on A in the excited state of less than 2 G or $2 \times 10^{-4} \text{ cm}^{-1}$. Reduction of A in excited state is due to partial cancellation of core polarization field by orbital hyperfine field.

¹⁴ A. A. Manenkov and A. M. Prokhorov, Zh. Eksperim. i Teor. Fiz. **31**, 346 (1956) [English transl.: Soviet Phys.—JETP **4**, 288 (1957)].

¹⁵ G. M. Zverev and A. M. Prokhorov, Zh. Eksperim. i Teor. Fiz. **34**, 513 (1958) [English transl.: Soviet Phys.—JETP **7**, 354 (1958)].

¹⁶ A survey of the systematics of hyperfine fields in the $3d$ ions is in preparation by one of us, S. Geschwind.

orbital h.f. field per unit spin is directly related to the g shift as indicated by Abragam and Pryce¹⁷ by the very simple expression

$$H_{h.f.}^{orb} = 2\mu_B \langle 1/r^3 \rangle \Delta g, \quad (7)$$

where μ_B is the Bohr magneton, $\langle 1/r^3 \rangle$ refers to the 3*d* electrons of the ion, and $\Delta g = |g| - 2.0023$. This may be written numerically as

$$H_{h.f.}^{orb} = 125 - \Delta g \langle 1/r^3 \rangle_{\text{atomic units}} \text{ kG}. \quad (8)$$

As Δg for $\bar{E} = +0.443$ and for the free Cr^{3+} , $\langle 1/r^3 \rangle = 3.958$ atomic units¹⁸ we find $H_{h.f.}^{orb} \approx +219\,000$ G, which almost cancels within the accuracy of measurement the $-195\,000$ -G core polarization field. The validity of Eqs. (7) and (8) is based on the assumption that the Δg is a manifestation of orbital effects only and arises from a perturbation term $\beta \mathbf{H} \cdot \mathbf{L}$ so that the correspondence with the orbital hyperfine interaction $\beta \beta_N \langle 1/r^3 \rangle \mathbf{I} \cdot \mathbf{L}$ may be made via Eq. (7). Equation (7) is not valid for that part of the g shift which would arise from the $2\beta \mathbf{S} \cdot \mathbf{H}$ term appearing in a perturbation expression. Sugano and Tanabe considered such terms in Eq. (6.18) of their paper, for example, terms of the type

$$\frac{\langle {}^2E | V_{\text{trig}} | {}^2T_2 \rangle \langle {}^2T_2 | 2S_z | {}^2T_2 \rangle \langle {}^2T_2 | \lambda \mathbf{L} \cdot \mathbf{S} | {}^2E \rangle}{[W({}^2E) - W({}^2T_2)]^2}. \quad (9)$$

However, the three such terms that appeared canceled each other so that to this order of perturbation theory Eq. (7) is valid for the 2E level.

We would expect that in the case of the \bar{E} state for V^{2+} in Al_2O_3 where Δg is half the value it is for Cr^{3+} ,¹⁹ a resolved hyperfine structure should be observed.

Note added in proof. This hfs has been observed. See S. Chinn, G. Devlin, F. Imbusch, and S. Geschwind, *Bull. Am. Phys. Soc.* (to be published).

V. SPIN-LATTICE RELAXATION IN \bar{E}

The spin-lattice relaxation time T_1 between the Zeeman components of \bar{E} is measured in the following way. The sample is continuously illuminated with Hg light to maintain an equilibrium population in the Zeeman levels of \bar{E} . At a fixed magnetic field, corresponding to resonance in \bar{E} for the microwave frequency used, a particular Zeeman component is monitored, for example line *A* in Fig. 3(a), with the high-resolution optical spectrometer and photomultiplier tube. As the microwaves are switched on, ions are transferred from the $(+1, -\frac{1}{2})$ to the $(-1, +\frac{1}{2})$ level reducing the intensity of line *A*. When the microwaves are switched

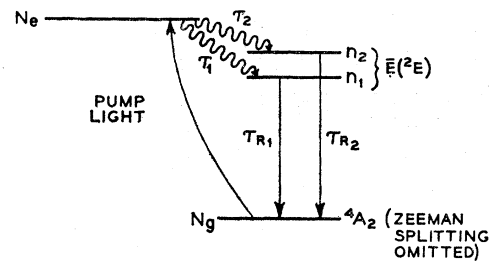


FIG. 8. Parameters used to describe recovery of intensity of line *A* (assumed proportional to n_1) after microwave saturation pulse is turned off. See Sec. Va of text.

off, the $(+1, -\frac{1}{2})$ level will recover to its initial population as shown in Fig. 3(b). This recovery time will depend on the spin-lattice relaxation time and the radiative lifetime as examination of the rate equations will now show.

a. Rate Equations Describing Relaxation Between Zeeman Levels of \bar{E}

To describe the recovery of the light signal after the microwave saturation pulse, we use a phenomenological model illustrated in Fig. 8. This model omits many of the details of the pumping cycle and radiationless transitions to the 2E level, etc., and limits itself to only those phenomenological aspects which are necessary to describe the recovery of the light signal *A* after the microwave pulse is turned off.

The *continuous* light pump is, even at its most intense value, such that in combination with the other parameters of the problem the population ($n_1 + n_2$) of the $\bar{E}({}^2E)$ state is orders of magnitude smaller than N_g , the population of the ground state. N_g , τ_1 , and τ_2 are the population and relaxation times of a hypothetical excited state from which the levels 1 and 2 are being filled. τ_1 and τ_2 are not necessarily equal since levels 1 and 2 may be populated at different rates. τ_{R1} and τ_{R2} are essentially the effective radiative lifetimes of levels 1 and 2 to the ground state and are indeed different as lines *A* and *D*, for example, are selectively reabsorbed at low temperatures. It is these effective lifetimes in the presence of reabsorption that one must consider rather than the lifetime in the absence of reabsorption such as would be measured in an optically thin crystal. This is so, as it is these effective lifetimes which determine the populations of levels 1 and 2 and correspondingly the intensity of light from these levels. Not only are τ_{R1} and τ_{R2} unequal but they are also temperature-dependent in the region of interest (1.5 to 4.2°K), reflecting the redistribution of population among the 4A_2 ground-state levels with temperature. In addition, τ_{R1} and τ_{R2} will depend upon concentration, geometry, method of viewing the light, and whether one is sitting on the peak or side of the optical line. Therefore, τ_{R1} and τ_{R2} must be measured *in situ* under identical conditions used in the microwave experiment. This

¹⁷ A. Abragam and M. H. L. Pryce, *Proc. Roy. Soc. (London)* **A205**, 135 (1951).

¹⁸ A. Freeman and R. E. Watson, in *Treatise on Magnetism*, edited by G. Rado and H. Suhl (Academic Press Inc., New York, to be published).

¹⁹ M. D. Sturge, *Phys. Rev.* **130**, 639 (1963).

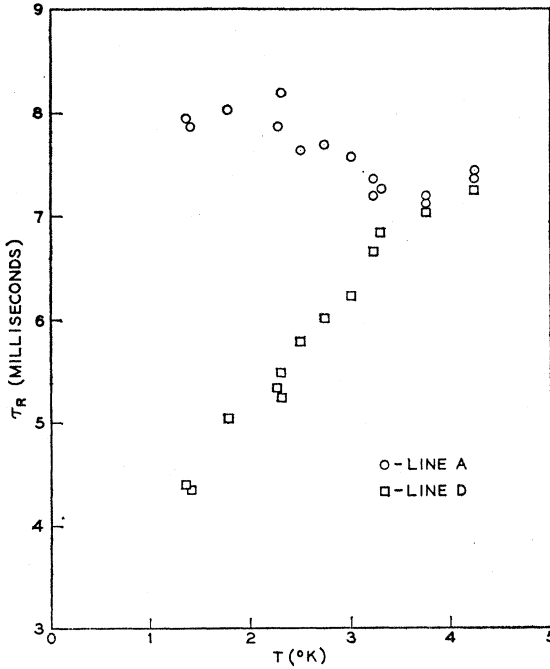


FIG. 9. Effective radiative lifetimes of lines A and D of Fig. 3(a) as a function of temperature. Change in selective reabsorption due to repopulation of ground state levels with temperature is responsible for different τ_R for A and D and variation with temperature.

was done in a separate experiment using a pulsed light source and the results are shown in Fig. 9 for a particular size sample, concentration, and spectrometer slitwidth. n_1 and n_2 are the populations, respectively, of the upper and lower Zeeman components of \bar{E} ; T_1 is the spin lattice relaxation between levels 1 and 2, and P_{12} is the rate of transitions between levels 1 and 2 induced by the microwave power. With these definitions, the rate equations for n_1 and n_2 are

$$\dot{n}_2 = -\frac{n_2}{\tau_{R2}} + \frac{N_e}{\tau_2} \frac{n_2 - (n_1 + n_2)\rho}{T_1} - (n_2 - n_1)P_{12}, \quad (10)$$

$$\dot{n}_1 = -\frac{n_1}{\tau_{R1}} + \frac{N_e}{\tau_1} \frac{n_1 - (n_1 + n_2)(1 - \rho)}{T_1} - (n_1 - n_2)P_{12}. \quad (11)$$

Here $\rho = e^{-\delta/2KT} / (e^{\delta/2KT} + e^{-\delta/2KT})$.

At equilibrium, $\dot{n}_1 = \dot{n}_2 = 0$ and adding Eqs. (10) and (11) we find

$$(n_2/\tau_{R2} + n_1/\tau_{R1}) = N_e(1/\tau_1 + 1/\tau_2). \quad (12)$$

(By equilibrium we mean, of course, equilibrium in the presence of the continuous light pump.) Thus, if $\tau_{R1} = \tau_{R2} = \tau_R$ then $n_1 + n_2 = \text{constant}$ at equilibrium independent of T_1 and P_{12} ; Eqs. (10) and (11) then reduce to first-order uncoupled equations. In this case the populations of n_1 and n_2 , after being disturbed by a microwave pulse, show an exponential recovery with a time constant τ given by

$$1/\tau = 1/\tau_R + 1/T_1. \quad (13)$$

However, if $\tau_{R1} \neq \tau_{R2}$ then $(n_1 + n_2)$ does depend on T_1 and P_{12} , and, in addition, will not be a constant during the recovery of the populations n_1 and n_2 towards equilibrium after the microwaves are shut off.

As we are only concerned with the individual development in time of n_1 and n_2 after the microwaves are shut off we may set $P_{12} = 0$ and we have the two coupled equations

$$\dot{n}_1 = n_1 \left(-\frac{1}{\tau_{R1}} - \frac{\rho}{T_1} \right) + n_2 \frac{(1 - \rho)}{T_1} + \frac{N_e}{\tau_1}, \quad (14)$$

$$\dot{n}_2 = n_1 \frac{\rho}{T_1} + n_2 \left(-\frac{1}{\tau_{R2}} - \frac{(1 - \rho)}{T_1} \right) + \frac{N_e}{\tau_2}, \quad (15)$$

whose solutions are

$$n_1 = c_1 e^{(\alpha + \lambda)t/2} + c_2 e^{(\alpha - \lambda)t/2} + n_1^{\text{eq.}} \quad (16)$$

$$n_2 = c_3 e^{(\alpha + \lambda)t/2} + c_4 e^{(\alpha - \lambda)t/2} + n_2^{\text{eq.}}, \quad (17)$$

where

$$\alpha = -\left(\frac{1}{\tau_{R1}} + \frac{1}{\tau_{R2}} \right) - \frac{1}{T_1}, \quad (18)$$

$$\beta = -\left[\frac{1}{\tau_{R1}\tau_{R2}} + \frac{\rho}{T_1} \left(\frac{1}{\tau_{R2}} - \frac{1}{\tau_{R1}} \right) + \frac{1}{T_1\tau_{R1}} \right], \quad (19)$$

$$\lambda = +(\alpha^2 + 4\beta)^{1/2}; \quad (20)$$

$n_1^{\text{eq.}}$ and $n_2^{\text{eq.}}$ are determined from (14) and (15) with $\dot{n}_1 = \dot{n}_2 = 0$; $c_1, c_2, c_3,$ and c_4 are constants determined by the initial conditions (i.e., degree of microwave saturation of levels 1 and 2). However, c_1/c_2 and c_3/c_4 are independent of initial conditions and are given by

$$\frac{c_1}{c_2} = \frac{[1/\tau_{R1} - \rho/T_1(\tau_{R2}/\tau_{R1} - 1) + 1/T_1(\tau_{R2}/\tau_{R1}) + \frac{1}{2}(\alpha - \lambda)]}{[1/\tau_{R1} - \rho/T_1(\tau_{R2}/\tau_{R1} - 1) + 1/T_1(\tau_{R2}/\tau_{R1}) + \frac{1}{2}(\alpha + \lambda)]}, \quad (21)$$

$$\frac{c_3}{c_4} = \frac{[1/\tau_{R2} - \rho/T_1(1 - \tau_{R1}/\tau_{R2}) + 1/T_1] + \frac{1}{2}(\alpha - \lambda)}{[1/\tau_{R2} - \rho/T_1(1 - \tau_{R1}/\tau_{R2}) + 1/T_1] + \frac{1}{2}(\alpha + \lambda)}. \quad (22)$$

Above 3.3°K, reference to Fig. 9 shows that $\tau_{R_1} \cong \tau_{R_2}$ so that the recovery time of the light signal will be adequately described by Eq. (13) instead of Eqs. (16)–(22). This is also true even at lower temperatures in the more dilute samples as reabsorption is less pronounced. In addition, of course, since above 3.3°K $T_1 \ll \tau_{R_1}$ or τ_{R_2} , the radiative correction becomes less significant and first-order corrections to Eq. (13) are often adequate so that one can avoid the complexity of Eqs. (16) through (22). However, at lower temperatures and in the more concentrated samples where $\tau_{R_1} \neq \tau_{R_2}$ and $T_1 \sim \tau_R$, it was necessary to trial fit the experimental results to Eqs. (16)–(22) to obtain the best T_1 .

b. Continuous Averaging Technique

Below the λ point of He, where microwave saturation of the Zeeman levels of \bar{E} is easier because of the longer T_1 , the change of intensity of line A can be as large as 10% so that the relaxation process could be easily observed as shown in Fig. 10(b) by connecting the output of the photomultiplier tube directly to the oscilloscope. However, at higher temperatures, the decrease in T_1 made it more difficult to saturate the transition (recall the small value of g_1). In addition, above the λ point the bubbling of the helium would produce a 10% noise modulation of the light signal so

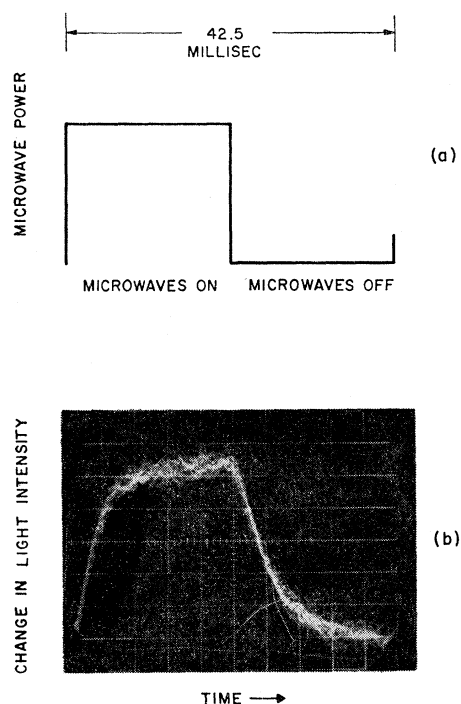


FIG. 10. (a) Square wave modulation of microwave signal. Upper portion of square wave corresponds to microwaves on and lower portion to microwaves off. (b) Recovery of light signal from a particular Zeeman component after microwaves are shut off, displayed directly on oscilloscope. Temperature is 1.6°K and change of light signal due to microwave saturation is approximately 5% of total.

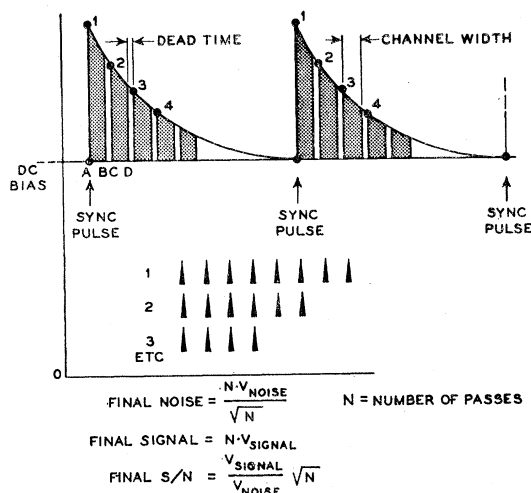


FIG. 11. Illustration of recovery of signal from noise with continuous averaging technique. See Sec. Vb of text.

that at times no signal at all was discernible on the oscilloscope as seen in Fig. 12(a).

To circumvent this difficulty, use was made of a continuous averaging technique described by Klein and Barton^{20,21} whereby the transient recovery cycle was averaged over several hundred thousand cycles to improve the signal to noise. As a general illustration of this technique, consider a repetitive phenomenon whose start each time is associated with some synchronization pulse as shown in Fig. 11. This same synchronization pulse starts a sequence of events in a multichannel analyzer as follows: The amplitude of the signal at point A in time is sampled and converted in an analog-to-digital converter (ADC) to a 4-Mc/sec pulse train whose duration (and therefore the number of pulses contained) is proportional to the amplitude at time A. The number of pulses in this train is then counted between times A and B (the channel width) and stored in the first channel (address) of a multichannel memory. There is a 12.5- μ sec dead time while the memory is switched to the second channel and the signal is again sampled at point C in time. Again the ADC produces a train of pulses whose number is proportional to the amplitude of the signal at time C and these are counted between C and D and stored in channel 2 of the memory, etc. This sequence of sampling the signal starts again

²⁰ M. P. Klein and G. W. Barton, Jr., in *International Conference on Paramagnetic Resonance (Jerusalem 1962)*, edited by W. Low (Academic Press Inc., New York, 1963, p. 698; Rev. Sci. Instr. 34, 754 (1963).

²¹ The basic idea behind the continuous averaging technique must go back at least as far as Lord Rayleigh. Nuclear physicists have been using it for years and the people who study the Mössbauer effect use it regularly. We have singled out Klein and Barton for special reference as the possibility of using it in our application was stimulated by their paper in Jerusalem in July, 1962 and subsequent discussions with Dr. Klein. Further references to the recent application to nmr and epr may be found in L. C. Allen and L. F. Johnson, *J. Am. Chem. Soc.* 85, 2668 (1963).

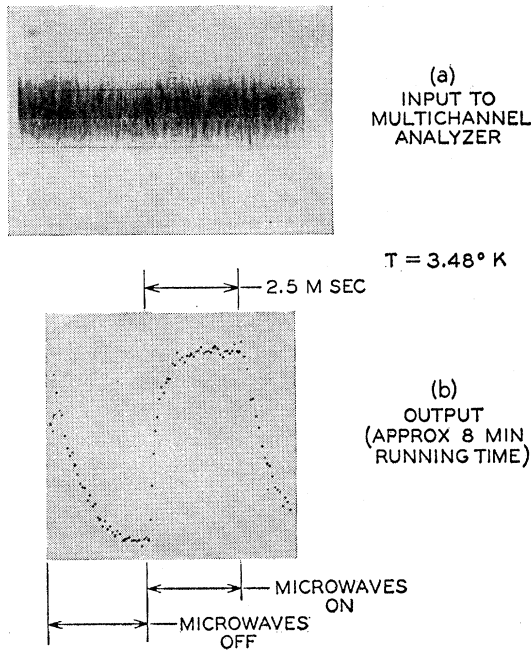


FIG. 12. (a) Light signal, modulated at microwave chopping frequency (200 cps), buried in noise. (b) Extraction of signal from noise after 8 min running time, corresponding to 96 000 samplings, giving an improvement in S/N of $96\,000 \approx 305$. Each dot represents a channel and its ordinate is proportional to the amplitude of the signal.

at the next synchronization pulse. The actual rms amplitude of the noise, V_{noise} may be much greater than the actual signal. However, on repeated samplings in any one channel, V_{noise} will appear with equal probability with either positive or negative sign. Therefore, after N samplings the accumulated rms noise signal will be $N^{1/2}V_{\text{noise}}$, i.e., a random walk in one dimension. The desired signal will, on the other hand, accumulate at a rate directly proportional to the number of passes N . Thus the final signal to noise will be improved by a factor of \sqrt{N} . To see what this amounts to, consider a 200-cps repetitive signal and an 8-min running time. In this case $N = 96\,000$ and $\sqrt{N} = 311$, so that we expect an improvement in signal to noise of approximately 300, resulting in the signal shown in Fig. 12(b). It is worth observing that this technique discriminates against low-frequency noise and drift since any drift caused by drift in lamp intensity, etc., which occurs in a time long compared to the repetition period is averaged out.

The \sqrt{N} improvement does not mean that if we make twice as many passes in the same time interval that we will increase the S/N by $\sqrt{2}$ at no other cost to us. For this would seem to violate the fact that improvement in S/N must go as $\sqrt{(\text{time})}$. The answer is that we assume that the time constant of the circuit that precedes the analyzer is of the order of the channel width time so as to keep the noise to a minimum consistent

with sufficient bandwidth to reproduce the signal. If we go twice as fast and change nothing else we distort our signal, if the time constant preceding the analyzer had been properly adjusted for the first rate of scan.

Each dot on the photograph in Fig. 12(b) represents a memory channel and its vertical position is proportional to the total number of counts accumulated per channel. Initially the data were actually printed digitally. More recently it has been punched on paper tape in binary coded decimal form and these tapes are processed by an IBM 7090 to yield a logarithmic plot of the light recovery signal versus time as shown in Fig. 13.

A block diagram of the system used in the continuous averaging technique is shown in Fig. 14. An RIDL 400 channel analyzer with internal ADC was used.²²

c. Features of Main Spin-Lattice Relaxation Processes

Before proceeding to a presentation of the results, we briefly cite the main well-known spin-lattice relaxation processes. Excellent detailed presentations of the subject may be found in many places.²³⁻²⁶ A theoretical

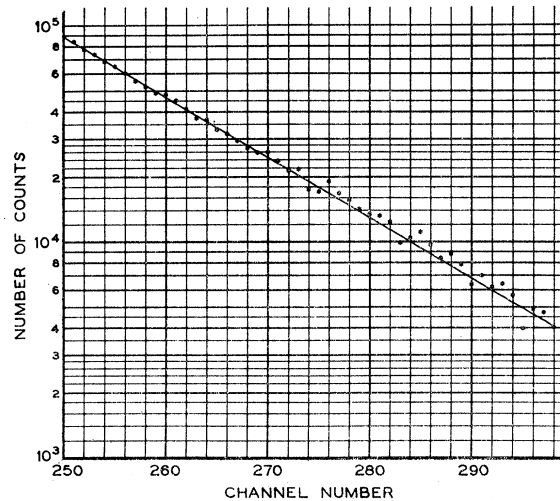


FIG. 13. Semilog plot of recovery of light signal when microwaves are switched off. Data are plotted by IBM 7090 from punched paper tape output of RIDL multichannel analyzer. Abscissa scale refers to channel number while ordinate scale refers to counts per channel modulo 10^6 . Time between channels in this figure is $112.5 \mu\text{sec}$, giving a recovery time at this temperature of 3.12°K of 1.75msec . This time has to be corrected for the radiative lifetime of \bar{E} to give T_1 as described in Sec. Va of text.

²² Radiation Instrument Development Laboratory Multichannel Analyzer, Model 34-12B. Multichannel analyzers suitable to this application are available from at least half a dozen other manufacturers.

²³ J. H. Van Vleck, Phys. Rev. **57**, 426 (1940).

²⁴ R. Orbach, Proc. Roy. Soc. (London) **A264**, 458 (1961).

²⁵ R. D. Mattuck and M. W. P. Strandberg, Phys. Rev. **119**, 1204 (1960).

²⁶ P. L. Scott and C. D. Jeffries, Phys. Rev. **127**, 32 (1962).

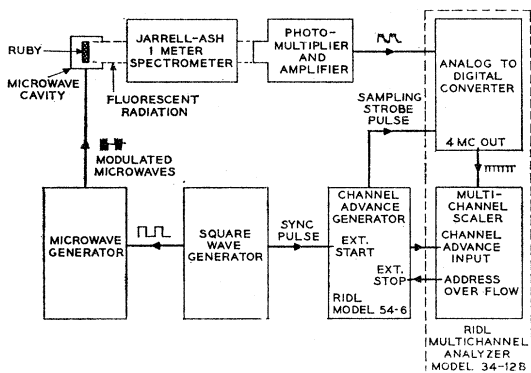


FIG. 14. Block diagram of continuous averaging technique used to measure T_1 in \bar{E} using an RIDL multichannel analyzer with ADC. In most runs only 100 to 200 channels of the 400 available were used. Filtering precedes the analog-to-digital converter whose time constant is roughly equal to a channel width.

study specifically related to the 2E state in ruby has been made earlier by Kiel.²⁷ However, there were some errors and omissions in Kiel's original approach. These have been corrected in a more accurate treatment by Orbach, Blume, Kiel, and Geschwind.²⁸

In the direct process the ion either emits or absorbs a phonon of frequency $\nu = \delta_1/h$ equal to the Zeeman splitting of the \bar{E} state. At the very lowest temperatures, the direct process will dominate as only these very low frequency phonons are thermally excited. As the temperature is raised and higher frequency phonons are made available, the indirect or two-step processes come into play. If there is a real excited state of the ion a distance Δ above our doublet, with Δ less than the Debye energy, we anticipate an Orbach process.²⁹ In this two-step process (see Fig. 4) the ion in level "b" absorbs a phonon of frequency approximately Δ and makes a transition to a real intermediate state a distance $\approx \Delta$ away and then emits a phonon of frequency $\Delta + \delta_1$ as it makes a transition from this intermediate state to level "a." Energy is conserved at each stage of this process. At still higher temperatures the Raman process enters in which the intermediate state is virtual and may lie at any distance above the ground state below the Debye frequency. Although the Raman process makes use of a large portion of the entire phonon spectrum, it is nonetheless a higher order process and so only becomes effective at higher temperatures where the phonon spectrum becomes very rich. The temperature and frequency dependence associated

²⁷ A. Kiel, *Advances in Quantum Electronics* (Columbia University Press, 1961), p. 417.

²⁸ M. Blume, R. Orbach, A. Kiel and S. Geschwind (to be published).

²⁹ C. B. P. Finn, R. Orbach, and W. P. Wolf, *Proc. Phys. Soc. (London)* **77**, 261 (1961).

with these three main processes are listed below:

$$\text{Direct process: } T_1 \propto 1/(\nu^4 T) \quad (\text{Kramers doublet}),$$

$$\text{Orbach process: } T_1 \propto e^{\Delta/KT},$$

$$\text{Raman process: } T_1 \propto T^9 \quad (\text{Kramers doublet}).$$

d. Experimental Results and Discussion

The recovery time τ of the intensity of line A after the turning off of a microwave saturation pulse is plotted in Fig. 15 as a function of temperature for a fairly dilute sample of ruby at 48 kMc/sec. The leveling off of τ at lower temperatures is due to the masking of the spin-lattice relaxation time T_1 by the radiative lifetime τ_R as described earlier. In Fig. 16, the corrections for the radiative lifetime have been made, as described in Sec. IVa, and T_1 of the \bar{E} level is plotted as a function of inverse temperature on a semilog plot for two different concentrations and at 24 and 48 kMc/sec.

It is seen that $T_1 = \text{const } e^{\Delta/KT}$ where $\Delta \approx 29 \text{ cm}^{-1}$. As this separation corresponds so well to the known separation of 29 cm^{-1} between the \bar{E} and $2\bar{A}$ levels as meas-

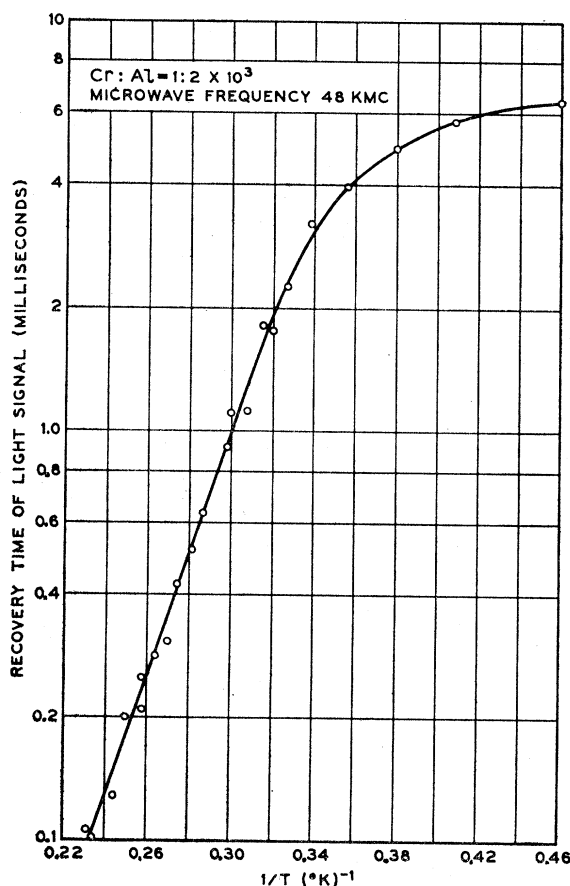


FIG. 15. Semilog plot of recovery time of light signal from an R_1 Zeeman component after microwave saturation pulse in \bar{E} is switched off. Leveling off of curve at low temperatures is due to masking of T_1 in \bar{E} by the radiative lifetime τ_R .

ured spectroscopically, it is immediately apparent that we are dealing with an Orbach process with $2\bar{A}$ as the intermediate state. Further evidence for this is the essential frequency or field independence of T_1 . As stated earlier the direct process, for example, would exhibit a $1/\nu^4$ behavior. The Orbach process should also be concentration-independent, which it is essentially seen to be over a range of concentrations varying by a factor of 10.

One would anticipate that at lower temperatures where T_1 due to the Orbach process becomes very long that one would begin to observe the direct process. However, while one can still observe a qualitative increase in τ with decreasing temperature below 2.8°K it becomes very difficult to extract *quantitatively* accurate values of T_1 as T_1 has become longer than τ_R with which it is in parallel [see Eq. (13)]. In addition, the optically produced 29-cm $^{-1}$ "hot phonons" to be discussed in Sec. VI affect T_1 at the lower temperatures. These effects must be explored in greater detail before one can say anything *quantitative* about the direct process, so that this paper limits itself essentially to the Orbach process.

e. Field Dependence of Orbach Process

Since Δ is very much greater than the Zeeman splitting, we do not expect to see a very significant dependence upon field or frequency for the Orbach process. However, it is interesting to examine just how large it might be for our range of fields. Referring to Fig. 4, let M_A be proportional to the spontaneous emission rate for the spin-flip transition from $2\bar{A}$ to \bar{E} by phonon emission and M_B the corresponding nonspin-flip rate.

$$W_1 = (w_{\text{up}} - w_{\text{down}})_{bc} = [\Delta - \frac{1}{2}(\delta_1 + \delta_2)]^3 M_A \{ N_b \bar{N}(\Delta - \frac{1}{2}(\delta_1 + \delta_2)) - N_c [\bar{N}(\Delta - \frac{1}{2}(\delta_1 + \delta_2)) + 1] \}, \quad (23a)$$

$$W_2 = (w_{\text{up}} - w_{\text{down}})_{bd} = [\Delta - \frac{1}{2}(\delta_1 - \delta_2)]^3 M_B \{ N_b \bar{N}(\Delta - \frac{1}{2}(\delta_1 - \delta_2)) - N_d [\bar{N}(\Delta - \frac{1}{2}(\delta_1 - \delta_2)) + 1] \}, \quad (23b)$$

$$W_3 = (w_{\text{up}} - w_{\text{down}})_{ac} = [\Delta + \frac{1}{2}(\delta_1 - \delta_2)]^3 M_B \{ N_a \bar{N}(\Delta + \frac{1}{2}(\delta_1 - \delta_2)) - N_c [\bar{N}(\Delta + \frac{1}{2}(\delta_1 - \delta_2)) + 1] \}, \quad (23c)$$

$$W_4 = (w_{\text{up}} - w_{\text{down}})_{ad} = [\Delta + \frac{1}{2}(\delta_1 + \delta_2)]^3 M_A \{ N_a \bar{N}(\Delta + \frac{1}{2}(\delta_1 + \delta_2)) - N_d [\bar{N}(\Delta + \frac{1}{2}(\delta_1 + \delta_2)) + 1] \}. \quad (23d)$$

\bar{N} is the Bose factor corresponding to the energy in parentheses.

$$dN_b/dt = -(W_1 + W_2), \quad (24a)$$

$$dN_a/dt = -(W_3 + W_4), \quad (24b)$$

$$dN_c/dt = (W_1 + W_3), \quad (24c)$$

$$dN_d/dt = (W_2 + W_4). \quad (24d)$$

Assuming that $(N_a + N_b + N_c + N_d)$ is constant, Eqs. (24) reduce to a set of three simultaneous linear first-order differential equations in three unknowns. As such, the return to equilibrium of the population of any of the levels will in general be described by three time constants. However, as $\Delta \gg kT$, $N_c + N_d \ll N_a$ or N_b , and if terms of order $(N_c + N_d)/(N_a + N_b)$ are neglected compared to unity we find that the recovery of the populations a and b may be expressed by a single time constant, i.e.,

$$-\frac{d}{dt}(N_b - N_a) = \frac{1}{T_1} [(N_b - N_a) - (N_b^{\text{eq.}} - N_a^{\text{eq.}})]$$

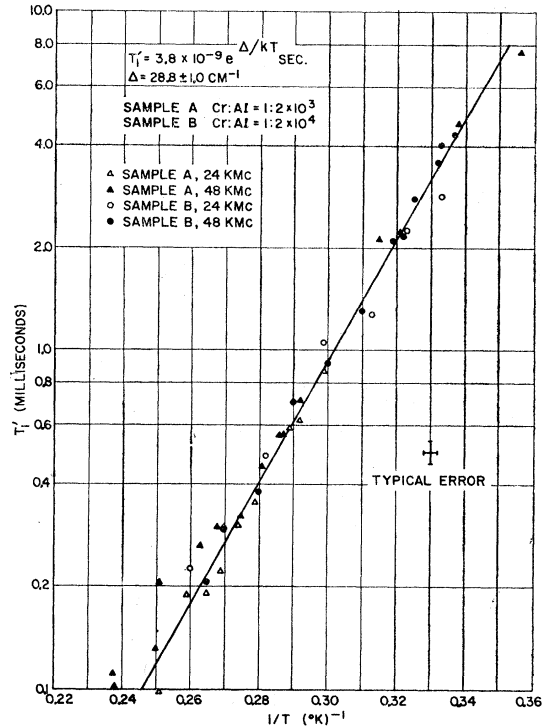


Fig. 16. Semilog plot of T_1 in \bar{E} versus $1/T$, showing Orbach relaxation with $T_1 = 3.8 \times 10^{-9} e^{\Delta/KT}$ sec and $\Delta = 28.8 \pm 1.0$ cm $^{-1}$. The constant 3.8×10^{-9} sec multiplied by four is the time for spontaneous decay from one Zeeman component of $2\bar{A}$ to \bar{E} with a spin flip and emission of a 29-cm $^{-1}$ phonon.

Then following Finn, Orbach, and Wolf²⁹ we write the following rate equations, where direct connections between a and b and between c and d are neglected:

with T_1 given by

$$T_1 = \left[\frac{M_A + M_B}{M_A M_B} \frac{1}{\Delta^3} e^{\Delta/kT} \right] / \left[4 \cosh \frac{\delta_1}{2kT} \cosh \frac{\delta_2}{2kT} + 4 \cosh \frac{\delta_1}{2kT} \sinh \frac{\delta_2}{2kT} \right. \\ \left. \times \left\{ \frac{3(\delta_1 + \delta_2)}{2\Delta} \left(\frac{M_A}{M_A + M_B} - 1 \right) + \frac{3}{2\Delta} (\delta_1 - \delta_2) \left(\frac{M_B}{M_A + M_B} - 1 \right) \right\} \right]. \quad (25)$$

The first correction term, $4 \cosh(\delta_1/2kT) \cosh(\delta_2/2kT)$ represents the effect of the Zeeman splitting in the exponential term on the Bose factor, whereas the second term, $4 \cosh(\delta_1/2kT) \sinh(\delta_2/2kT)$, \dots , is the effect of the Zeeman splitting on the Δ^3 or density of states term. As $\delta/\Delta \ll 1$, this second correction term, connected with the Δ^3 factor, is negligible compared to the first term associated with the Boltzmann factor, so that

$$T_1 \sim \frac{M_A + M_B}{4M_A M_B} \frac{1}{\Delta^3} e^{\Delta/kT} / \left[\cosh \frac{\delta_1}{2kT} \cosh \frac{\delta_2}{2kT} \right]. \quad (26)$$

The Zeeman splitting correction to the usual exponential temperature dependence of T_1 in the Orbach process, given by the denominator of Eq. (26) will be important only when the Zeeman splitting becomes comparable to kT . At 48 kMc/sec and at the lowest temperatures shown in Fig. 16, this correction amounts to 10%. Therefore we do not expect a magnetic field or frequency dependence any greater than this in the range of temperature covered in Fig. 16. However, this correction was made for the low-temperature points (approx. 3.2 to 2.8°K) and is included in Fig. 16 so that in effect the ordinate being plotted is $T_1 \cosh(\delta_1/2kT) \times \cosh(\delta_2/2kT)$, which we call T_1' .

f. Lifetime of $2\bar{A}$ Level

It is important to note that the constant which appears in front of the exponential factor in the Orbach process is the time for spontaneous decay from $2\bar{A}$ to \bar{E} with emission of a 29-cm⁻¹ phonon. However, as was mentioned earlier, one expects two different rates of spontaneous emission of a phonon corresponding very roughly to the "spin-flip" and "nonspin-flip" transitions from $2\bar{A}$ to \bar{E} . It is easy to show that it is the slower of these two rates that appears as the coefficient in the Orbach process. Referring to Fig. 4 we see that the rate for a *single* ion to go from b to a via the intermediate states is given by

$$w_{ba} = w_{bc} \times (\text{time spent in } c) \times w_{ca} + w_{bd} \\ \times (\text{time spent in } d) \times w_{da}, \quad (27)$$

$$w_{ba} = w_{bc} w_{ca} / w_{cb} + w_{ca} + w_{bd} w_{da} / w_{db} + w_{da}. \quad (28)$$

Similarly w_{ab} is given by

$$w_{ab} = w_{ac} w_{cb} / w_{ca} + w_{cb} + w_{ad} w_{db} / w_{da} + w_{db}. \quad (29)$$

Now $w_{ac}/w_{ca} = \bar{n}_{ac}/(\bar{n}_{ac} + 1) \simeq \bar{n}_{ac}$ since $\bar{n} \ll 1$, etc., where

$$\bar{n}_{ij} = (e^{(E_j - E_i)/kT} - 1)^{-1}.$$

Assume that (for what are essentially the spontaneous emission rates since $\bar{n} \ll 1$) $w_{ca} = w_{ab}$, $w_{cb} = w_{da}$, i.e., that the nonspin-flip matrix elements are equal and that the spin-flip matrix elements are equal and that the density of states factor Δ^3 is the same for all the transitions. Then again neglecting the populations of c and d compared to a and b we have

$$1/T_1 = w_{ab} + w_{ba} = w_{cb} w_{ca} / (w_{ca} + w_{cb}) \\ \times [\bar{n}_{ac} + \bar{n}_{ad} + \bar{n}_{bc} + \bar{n}_{bd}]. \quad (30)$$

or

$$1/T_1 = w_{cb} w_{ca} / (w_{ca} + w_{cb}) \\ \times e^{-\Delta/kT} [4 \cosh(\delta_1/2kT) \cosh(\delta_2/2kT)]. \quad (31)$$

If $w_{cb} \ll w_{ca}$, we see that $w_{cb} w_{ca} / (w_{ca} + w_{cb}) \rightarrow w_{cb}$. Conversely if $w_{ca} \ll w_{cb}$, this ratio approaches w_{ca} , i.e., it is the slower of the two rates that appears as the coefficient in the Orbach process. This result is of course apparent from Eq. (26) as well, which is identical to Eq. (31), but in which the density of states factor Δ^3 has been included in the w 's. In Ref. 28 it is shown that it is the spin-flip transition which is the slower, i.e., $w_{da} = w_{cb} \ll w_{ab} = w_{ca}$. If we write $w_{da} = 1/T_{2\bar{A} \rightarrow \bar{E}-}$, where $+$ and $-$ refer to $m_s = +\frac{1}{2}$ and $-\frac{1}{2}$, respectively, then

$$T_1 = \frac{1}{4} T_{2\bar{A} \rightarrow \bar{E}-} e^{\Delta/kT}. \quad (32)$$

Experimentally we find $\frac{1}{4} T_{2\bar{A} \rightarrow \bar{E}-} = 3.8 \times 10^{-9}$ sec. We will show below that this is close to what is predicted by a rough theoretical estimate. This number is in excellent agreement with the more detailed analysis in Ref. 28 where it is also shown that $T_{2\bar{A} \rightarrow \bar{E}+}$ is approximately 50 times faster or approximately 3×10^{-10} sec. This predicts a lifetime broadening of the $2\bar{A}$ level of approximately 0.017 cm⁻¹. As this figure is by no means negligible compared to the observed linewidths of R_1 at low temperatures whose linewidth is due to random crystal strains (lifetime broadening of R_1 is insignificant as $\tau_R \approx 3 \times 10^{-3}$ sec), one might expect to observe a slightly wider line for R_2 compared to R_1 . Indications of this have been observed by McCumber and Sturge.³⁰

This lifetime of the $2\bar{A}$ level would result in an epr linewidth of approximately 0.2 kG in this level which in combination with the difficulty of saturating would make it very difficult to observe.

The lifetime of the $2\bar{A}$ level against spontaneous emission of a 29-cm⁻¹ phonon and decay to the \bar{E} level will play an important role in the discussion in Sec. VI

³⁰ D. E. McCumber and M. D. Sturge, J. Appl. Phys. **34**, 1682 (1963).

of the bottlenecking of the 29-cm^{-1} phonons produced by the light pump.

g. Estimate of $T_{2\bar{A} \rightarrow \bar{E}}$ from Static Strain on R Lines

It is interesting to estimate $T_{2\bar{A} \rightarrow \bar{E}}$ from the static strain data on the R lines and compare this estimate with the observed values of $4 \times 3.8 \times 10^{-9}$ sec.

The electrostatic potential energy at a paramagnetic center may be expanded in powers of the local strain ϵ :

$$V = V^0 + V^{(1)}\epsilon + V^{(2)}\epsilon^2 + \dots, \quad (33)$$

V^0 is the static term in the absence of strain. $V^{(1)}\epsilon$ is the first-order change in potential energy due to the strain and is the orbit-lattice operator which is responsible for phonon assisted transitions between electronic states when ϵ is the dynamic strain produced by the thermal phonons. $V^{(1)}$ operates on the coordinates of the electrons and ϵ is a lattice or phonon operator. The transition rate from $2\bar{A}$ to \bar{E} with emission of a phonon will then be given by first order time-dependent perturbation theory as

$$w_{2\bar{A} \rightarrow \bar{E}} = \frac{2\pi}{\hbar} |\langle \bar{E}' | V^{(1)} | 2\bar{A}' \rangle|^2 |\langle n+1 | \epsilon | n \rangle|^2 \rho_E, \quad (34)$$

where ρ_E is the density of states at 29cm^{-1} in the acoustic phonon spectrum. The primes have been placed on $2\bar{A}$ and \bar{E} to designate these states as modified by the admixture of the 2T_2 by s-o coupling and trigonal field. Without this admixture there are no matrix elements of the appropriate orbital operators \tilde{V} in the pure ${}^2E(t_2^3)$ state, as shown in Ref. 28. Actually $V^{(1)}\epsilon$ is a tensor dot product^{31,32} $\tilde{V}^{(1)}:\tilde{\epsilon}$

$$\tilde{V}:\tilde{\epsilon} = \sum_{\Gamma,\gamma} V(\Gamma)c(\Gamma,\gamma)\epsilon(\Gamma,\gamma), \quad (35)$$

where Γ refers to an irreducible representation of the point group at the paramagnetic site, γ is one of the basis vectors of Γ and $c(\Gamma,\gamma)$ are combinations of the spherical harmonics appropriate to the site symmetry; $\epsilon(\Gamma,\gamma)$ are those linear combinations of the strains which transform as $c(\Gamma,\gamma)$. It is customary to attempt an estimate of the orbital operator matrix element in Eq. (34) by reference to the experimentally observed shifts in energy levels with static strain.

The change in splitting between the $2\bar{A}$ and \bar{E} levels with static strain measured by Schawlow³³ involves diagonal elements of the perturbing potential in \bar{E}' and $2\bar{A}'$, i.e.,

$$V\epsilon \sim 2 |\langle 2\bar{A}'_{\pm} | \tilde{V} | 2\bar{A}'_{\pm} \rangle| \epsilon = 2 |\langle \bar{E}'_{\pm} | \tilde{V} | \bar{E}'_{\pm} \rangle| \epsilon, \quad (36)$$

where ϵ is some average strain. Schawlow finds $V\epsilon = 0.055\text{ cm}^{-1}$ for a stress of 10^9 dyn/cm^2 along the c

axis. Using the elastic compliance constant $S_{33} \sim 0.2 \times 10^{-12}\text{ cm}^2/\text{dyn}$ to extract an average strain we find $V \approx 200\text{ cm}^{-1}$. One can hope for a rough estimate of $w_{2\bar{A} \rightarrow \bar{E}}$ by assuming that

$$|\langle \bar{E}' | \tilde{V} | 2\bar{A}' \rangle| \sim |\langle 2\bar{A}' | \tilde{V} | 2\bar{A}' \rangle|. \quad (37)$$

Such an assumption will generally be valid within an order of magnitude and is especially good for our case as shown in a detailed examination of the problem by Blume, Orbach, Kiel, and Geschwind²⁸ who find that

$$|\langle \bar{E}'_{\pm} | \tilde{V} | 2\bar{A}'_{\pm} \rangle| \gg |\langle \bar{E}'_{\pm} | \tilde{V} | 2\bar{A}'_{\mp} \rangle| \approx |\langle 2\bar{A}'_{\pm} | \tilde{V} | 2\bar{A}'_{\pm} \rangle|. \quad (38)$$

Here $+$ and $-$ refer to the two spin states. In effect the expression (38) shows that the spin-flip transition from $2\bar{A}$ to \bar{E} is slower than the nonspin-flip transition and that the matrix element of this slower path is approximately equal to the relevant matrix element which appears in the static strain experiment on the displacement of the R lines. We saw earlier that it is the slower of the two rates from $2\bar{A}$ to \bar{E} which appears as the constant multiplying the exponential in the Orbach process. We may therefore set $|\langle \bar{E}'_{\pm} | \tilde{V} | 2\bar{A}'_{\mp} \rangle| = V = 200\text{ cm}^{-1}$ in Eq. (34). The evaluation of Eq. (34) then proceeds in the well-known fashion^{23,24} for the direct process. We use an isotropic approximation for our estimate assuming equal velocities for longitudinal and transverse modes and use an average strain ϵ . In addition, we assume that 29 cm^{-1} is sufficiently below the Debye acoustic cutoff so that we may neglect dispersion and set $v = \omega/k$. Then substituting into Eq. (34)

$$\rho_E = 12\pi v^2 / v^3 h \quad \text{and} \quad |\langle n+1 | \epsilon | n \rangle|^2 = \hbar(n+1)k^2 / 2M\omega, \quad (39)$$

we find, since $n \ll 1$,

$$w_{2\bar{A} \rightarrow \bar{E}} = 24V^2 v_0^3 \pi^3 / \hbar v^5 \rho. \quad (40)$$

Taking $V = 200\text{ cm}^{-1}$; $v_0 = 10^{12}\text{ cps}$; $\rho = 4\text{ g/cm}^3$; and $v \approx 8 \times 10^5\text{ cm/sec}$, we find $w_{2\bar{A} \rightarrow \bar{E}} \approx 1.5 \times 10^8\text{ sec}^{-1}$, as compared to the experimental value of $0.6 \times 10^8\text{ sec}^{-1}$. Such good agreement is to be regarded as fortuitous in view of the rough approximations used, but is indicative of the good order of magnitude agreement that one can usually anticipate by this rough approximation of the necessary matrix element from strain data.³⁴ A more detailed application of the approach of Blume *et al.* as given in Ref. 28 indeed shows equally good agreement and is of course far more reliable.

VI. OPTICAL GENERATION OF 29 cm^{-1} (10^{12} cps) ACOUSTIC PHONONS

It was observed that below approximately 2.8°K the relaxation time T_1 , in \bar{E} , decreased with increasing light

³¹ M. Blume and R. Orbach, Phys. Rev. **127**, 1587 (1962).

³² A. L. Schawlow, A. H. Piksis, and S. Sugano, Phys. Rev. **122**, 1469 (1961).

³³ A. L. Schawlow, in *Advances in Quantum Electronics* (Columbia University Press, New York, 1961), p. 50.

³⁴ P. G. Klemens, Appl. Phys. Letters **2**, 81 (1963). Our procedure is identical to that used by Klemens in estimating the decrease in thermal conductivity of ruby when the 2E level is populated. Our value of $V \approx 200\text{ cm}^{-1}$ is more accurate than the value 10^8 cm^{-1} used by Klemens.

intensity. A microwave susceptibility technique that could measure relative changes in sample temperature as small as 10^{-3} deg Kelvin was used to establish that this decrease in T_1 was not a heating effect due to the higher light intensity.

Secondly, it was noticed that at the highest light intensity that was conveniently accessible, T_1 was independent of temperature below 2.8°K (the correction of course having been made for the radiative lifetime).

It is suggested that these effects are due to T_1 being controlled by 29-cm^{-1} phonons produced by the continuous pumping light in the decay of R_2 to R_1 , rather than by the thermal background of 29-cm^{-1} phonons. We now wish to examine this possibility that the 29-cm^{-1} phonons (10^{12} cps), which are emitted in the spontaneous transition of the Cr^{3+} ion from $2\bar{A}$ to \bar{E} level in the optical pumping cycle, are "bottlenecked" at low temperatures. As is well known,³⁵ by this is meant that these phonons do not come into thermal equilibrium with the bath (or to phonons of other energy) rapidly enough so that the phonon occupation number \bar{n} at this frequency is greater than its equilibrium value corresponding to the bath temperature. In effect, one has a narrow band of "hot phonons" around 29 cm^{-1} corresponding to a temperature $T_{\text{ph}} > T_{\text{bath}}$.³⁶

Let us assume that both \bar{E} and $2\bar{A}$ are populated at equal rates from levels above. Then since at very low temperatures (1.5°K) one finds virtually all the ions in the \bar{E} level, we may conclude that roughly half the ions in the \bar{E} level have arrived there via the $2\bar{A}$ level accompanied by the spontaneous emission of a phonon. If we designate by n_1 the equilibrium population of \bar{E} , then the rate at which \bar{E} is being filled from the $2\bar{A}$ level must be equal to $n_1/2\tau_R$ where τ_R is the radiative lifetime to the 4A_2 ground state. If we call τ_{ph} , the lifetime of the emitted phonons and N_{ph} their dynamic equilibrium number, then at dynamic equilibrium

$$n_1/2\tau_R = N_{\text{ph}}/\tau_{\text{ph}}. \quad (41)$$

The lifetime τ_{ph} is quite distinct from the lifetime of the $2\bar{A}$ level and could be considerably longer than it. At these very low temperatures, judging from thermal conductivity data,³⁷ we expect τ_{ph} of the transverse acoustic phonons to be limited by boundary scattering only and, therefore, might be as long as 10^{-6} sec. Recent theoretical work of Orbach and Vredevoe,³⁸ indicates that the lowest (transverse) branch of the phonon spectrum has an anomalously long lifetime for $\hbar\omega \gg kT$. These phonons decay by boundary scattering which converts them to other modes (longitudinal) which decay more rapidly. However, we will adopt a more conservative value of $\tau_{\text{ph}} \approx 10^{-7}$ sec. Our sample had 10^{17} Cr^{3+} ions

³⁵ J. H. Van Vleck, Phys. Rev. **59**, 724 (1941); **59**, 730 (1941).

³⁶ We wish to thank K. Dransfeld for the earliest discussions of this possibility prior to our accidental encounter with this phonon bottleneck in our experiments.

³⁷ M. G. Holland, J. Appl. Phys. **33**, 2910 (1962).

³⁸ R. Orbach and L. A. Vredevoe, Physics **1**, 90 (1964).

and let us assume that even for intense pumping light only 1 part in 10^4 are in the excited state, so that $n_1 = 10^{13}$. Since $\tau_R \approx 3.5 \times 10^{-3}$ sec, we find $N_{\text{ph}} \approx 10^{18}$. To find the average excitation \bar{n}_{opt} per mode corresponding to these optically generated acoustic phonons, we must divide N_{ph} by the total number of acoustic modes (using the Debye approximation) in the bandwidth ΔE into which these phonons are being emitted, i.e.,

$$\bar{n}_{\text{opt}} = \frac{N_{\text{ph}}}{9N(E/E_D)^3 \Delta E/E}. \quad (42)$$

Here E_D is the Debye energy of the acoustic modes and is approximately 300 cm^{-1} ³⁹; $N = 10^{20}$, the total number of unit cells in our sample; $E \approx 30\text{ cm}^{-1}$; ΔE is determined by the total lifetime of the $2\bar{A}$ level which we saw in Sec. V was 3×10^{-10} sec as determined from the Orbach process so that $\Delta E/E \approx 2 \times 10^{-3}$. We therefore find that $\bar{n}_{\text{opt}} \approx 10^{-7}$. But since the thermal background at this energy of 29 cm^{-1} at 1.5°K is $\bar{n}_{\text{thermal}} \approx 10^{-12}$, \bar{n}_{opt} is some five orders of magnitude larger than \bar{n}_{thermal} and $\bar{n}_{\text{opt}} \approx 10^{-7}$ actually corresponds to an n_{thermal} of 2.6°K . \bar{n}_{opt} could easily be an order of magnitude larger than our estimate.

In effect therefore the Orbach relaxation at high light intensity is being controlled up to approximately 2.8°K by an optically generated spike in the phonon spectrum at 29 cm^{-1} . Above a lattice temperature of 2.8°K , the thermal phonons will dominate again, explaining the two experimental facts alluded to at the beginning of this section. We have only briefly mentioned these experimental results, as the effects of these optically generated phonons form a large topic in themselves and will be treated in a separate publication. The data on the Orbach process presented in this paper in Sec. V is in the regime of low light intensity where the effects of these optically produced phonons may be neglected.⁴⁰

ACKNOWLEDGMENTS

We wish to thank Miss B. B. Cetlin for computational aid; J. P. Remeika for growing the Al_2O_3 crystals doped with enriched Cr^{53} ; and M. P. Klein and W. Blumberg for advice with regard to the continuous averaging technique.

We also wish to acknowledge the very many stimulating and helpful discussions with many of our colleagues including M. Blume, K. Dransfeld, A. Kiel, M. Lax, W. B. Mims, R. Orbach, M. D. Sturge, and L. R. Walker.

³⁹ M. D. Sturge and D. E. McCumber (private communication) have arrived at this figure from an analysis of the vibrational satellites of the R lines. The exact θ_D will not be terribly important in any event, as one is producing orders of magnitude increase in the 29-cm^{-1} phonons.

⁴⁰ Failure to consider the effect of these optically produced 29-cm^{-1} phonons casts doubt on the meaningfulness of the T_1 's reported earlier at 1.6°K (Ref. 5). This would apply to Ref. 5 as well as the work of W. H. Culver, R. A. Satten, and C. R. Viswanathan, J. Chem. Phys. **38**, 775 (1963).

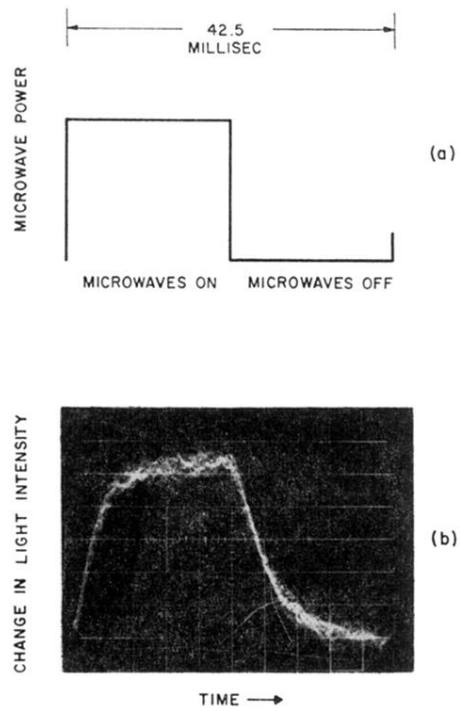


FIG. 10. (a) Square wave modulation of microwave signal. Upper portion of square wave corresponds to microwaves on and lower portion to microwaves off. (b) Recovery of light signal from a particular Zeeman component after microwaves are shut off, displayed directly on oscilloscope. Temperature is 1.6°K and change of light signal due to microwave saturation is approximately 5% of total.

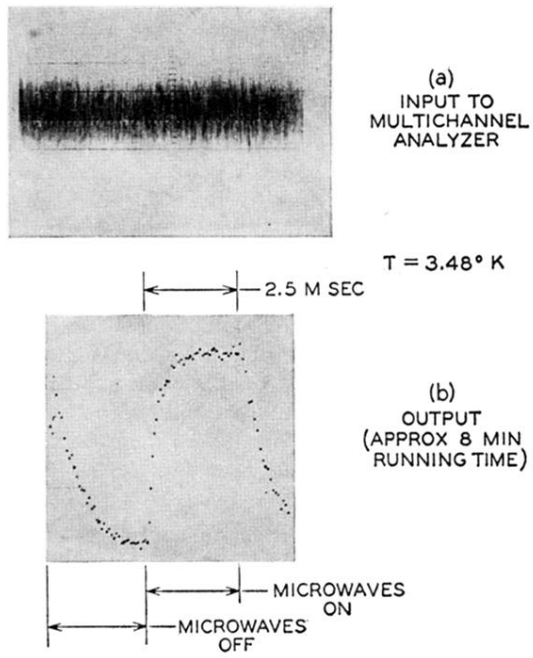


FIG. 12. (a) Light signal, modulated at microwave chopping frequency (200 cps), buried in noise. (b) Extraction of signal from noise after 8 min running time, corresponding to 96 000 samplings, giving an improvement in S/N of $96\,000 \approx 305$. Each dot represents a channel and its ordinate is proportional to the amplitude of the signal.

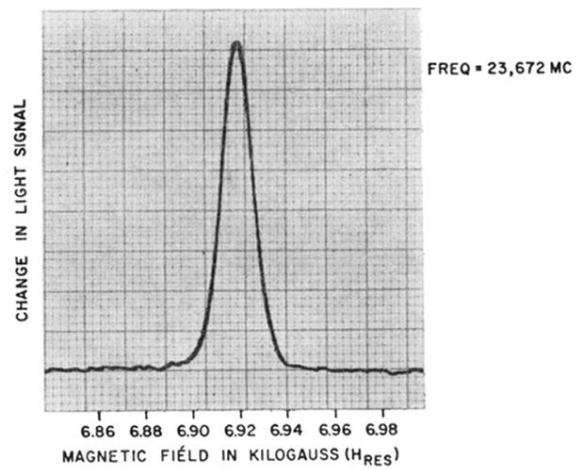


FIG. 6. Epr signal observed by optical detection in \vec{E} at 1.6°K from approximately 10^{11} spins in \vec{E} .

92% ENRICHED Cr^{53} IN Al_2O_3 ($\text{Cr}:\text{Al} \sim 1:10^3$)

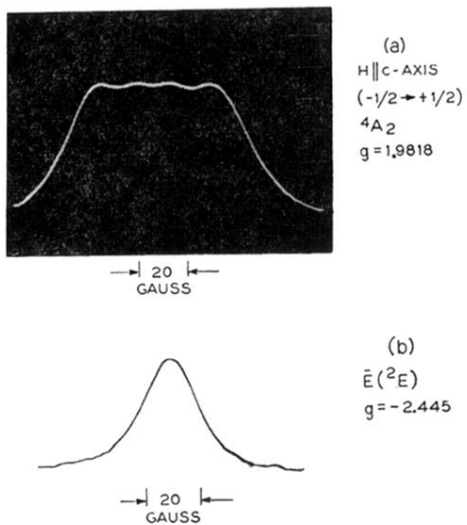


FIG. 7. Top figure shows epr signal from $-1/2 \rightarrow +1/2$ transition of $4A_2$ ground state in sample enriched with Cr^{53} . The hyperfine constant is approximately 20 G (separation between h.f. components). Lower figure shows resonance observed in same sample with no resolved hfs apparent. One may place an upper limit on A in the excited state of less than 2 G or $2 \times 10^{-4} \text{ cm}^{-1}$. Reduction of A in excited state is due to partial cancellation of core polarization field by orbital hyperfine field.